JOURNAL OF GEOPHYSICAL RESEARCH, VOL. 116, A08221, doi:10.1029/2011JA016499, 2011

Modeling the evolution of chorus waves into plasmaspheric hiss

J. Bortnik,[1] L. Chen,[1] W. Li,[1] R. M. Thorne,[1] and R. B. Horne[2]

Received 26 January 2011; revised 4 May 2011; accepted 16 May 2011; published 24 August 2011.

[1] Plasmaspheric hiss (PH) is a band-limited, incoherent whistler mode emission found predominantly in the plasmasphere or high-density plasma regions in the near-Earth space environment. Since its discovery in the late 1960s, PH has been recognized as playing an important role in shaping the structure and dynamics of the Earth's electron radiation belts and creating the slot region that separates the inner and outer belts. However, the origin of PH has been a topic of intense debate for over four decades. Here we present a model for the origin of PH that involves the evolution of chorus waves into the PH spectrum. We perform extensive ray tracing using the HOTRAY code and calculate Landau damping using newly developed suprathermal flux maps from THEMIS observations, that are L and magnetic local time dependent, for both inside and outside the plasmasphere. Our results show remarkable consistency with the observed statistical characteristics of hiss, including the day/night asymmetry in wave power, frequency spectrum, geomagnetic control of PH, quasi-parallel equatorial wave normal angles, and confinement within the plasmasphere. Our model also reproduces ancillary features such as exohiss and extremely low frequency (ELF) hiss and might be related to a previously reported phenomenon called lower hybrid resonance duct trapping in the ionosphere. A detailed analysis of ray morphologies shows a separation into four distinct groups, which correspond to (1) rays that are trapped at the plasmapause, (2) PH rays, (3) ELF hiss rays, and (4) rays that represent the bulk of the chorus ray power.

Citation: Bortnik, J., L. Chen, W. Li, R. M. Thorne, and R. B. Horne (2011), Modeling the evolution of chorus waves into plasmaspheric hiss, *J. Geophys. Res.*, *116*, A08221, doi:10.1029/2011JA016499.

1. Introduction

[2] Plasmaspheric hiss (PH) is a naturally occurring, electromagnetic plasma wave that propagates in the so-called whistler mode, i.e., R mode, with wave frequencies $f_{cH} < f < f_{ce}$, where f_{cH} and f_{ce} are the local proton and electron gyrofrequencies, respectively [*Thorne et al.*, 1973]. As its name suggests, PH is an incoherent, structureless emission (Figure 1a) that is generally confined within the plasmasphere (from $L \sim 1.6$ to the plasmapause), regions of high-density plasma in the near-Earth space environment such as plasmaspheric drainage plumes [*Chan and Holzer*, 1976; *Cornilleau-Wehrlin et al.*, 1978; *Hayakawa et al.*, 1986; *Parrot and Lefeuvre*, 1986], and possibly a high-latitude dayside plume region [*Russell et al.*, 1969]. Previous studies have shown that PH typically spans the frequency range between ~100 Hz and 2 kHz, although it may extend to several kHz at lower power levels [*Hayakawa and Sazhin*, 1992], with broadband amplitudes that are controlled by the level of geomagnetic activity, and range from ~10 pT during quiet times, to >100 pT during active periods [*Smith et al.*, 1974; *Thorne et al.*, 1974, 1977; *Meredith et al.*, 2004]. Although PH occurs at essentially all magnetic local times (MLT) and latitudes within the plasmasphere, there is nevertheless a pronounced MLT asymmetry in wave power, with dayside values being roughly an order of magnitude larger than those on the nightside [*Meredith et al.*, 2004, 2006].

[3] Although a variety of electromagnetic "hisses" have been observed with ground-based instruments and reported in the literature starting from the late 1950s [e.g., *Ellis*, 1959] (see also reviews by *Hayakawa and Sazhin* [1992] and *Bortnik et al.* [2009b]), it is important to distinguish PH as an emission that is only observed in space; that is, it was discovered and observed with the first high-altitude spacecraft [*Dunckel and Helliwell*, 1969; *Russell et al.*, 1969] and named "plasmaspheric hiss" in large part due to its *in situ* measurement within the plasmasphere [*Thorne et al.*, 1973]. This distinction is necessary because the hiss observed at a given point on the ground is a superposition of electromagnetic wave energy in the extremely low frequency (ELF) and very low frequency (VLF) bands, that arrives from different sources and locations on the ground and in space. Consequently, studies performed with ground-based and low-altitude satellite data in the 1960s and 1970s showed a variety of hiss morphologies, and different nomenclatures arose in an attempt to differentiate hiss according to its properties. For example, hiss was divided into

[1]Department of Atmospheric and Oceanic Sciences, University of California, Los Angeles, California, USA.
[2]British Antarctic Survey, Cambridge, UK.

0148-0227/11/2011JA016499

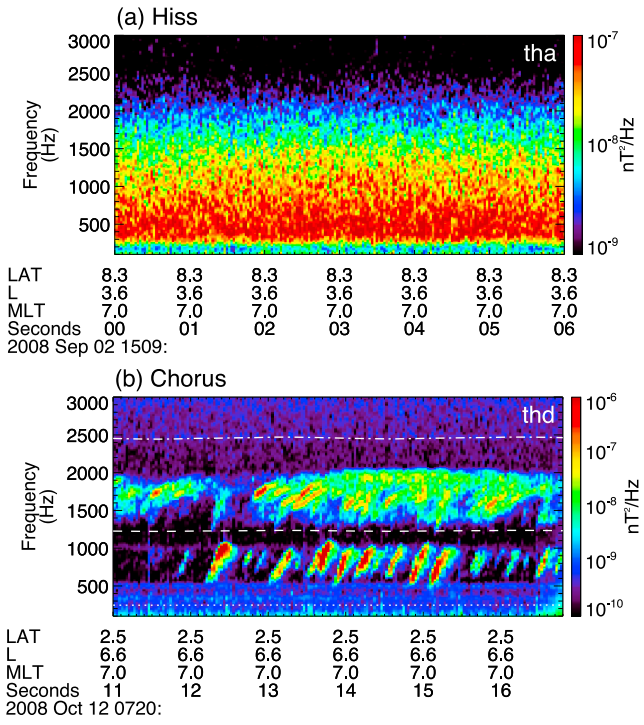

Figure 1. A typical example of (a) plasmaspheric hiss and (b) whistler mode chorus waves observed on the THEMIS spacecraft, inside and outside the plasmasphere, respectively. Both examples are shown on the same time scale (6 s total) and frequency range (0.1–3 kHz) at MLT = 7. The three white lines in Figure 1b represent 1 (dash-dotted), 0.5 (dashed), and 0.1 (dotted) f_{ce}^{eq}. The individual chorus elements are a factor of ~10 more intense than the hiss.

"daytime" and "nighttime" events [*Harang*, 1968], "steady state" and "disturbed" hiss [*Hayakawa et al.*, 1975], "morning side" and "evening side" events [*Hayakawa et al.*, 1977], "narrowband 5 kHz hiss" [*Ondoh et al.*, 1980, 1981], "a steady hiss" and a hiss with a latitude-dependent upper cutoff frequency [*Ondoh et al.*, 1982, 1983], lower hybrid resonance (LHR) and S-type hiss [*Gross and Larocca*, 1972], ELF hiss [*Gurnett and O'Brien*, 1964], as well as auroral and midlatitude hisses [*Ellis*, 1959]. In contrast, PH has a fairly consistent morphology, with well-defined characteristics as outlined above, and it is this specific emission which is the focus of the present study.

[4] Soon after its discovery, PH was recognized as playing a vital role in controlling the overall structure and dynamics of the Earth's radiation belts. Specifically, resonant pitch angle scattering of energetic electrons by PH largely accounts for the formation of the slot region that separates the inner ($1.3 < L < 2.5$) and outer ($3 < L < 7$) radiation belts [*Lyons et al.*, 1972; *Lyons and Thorne*, 1973; *Albert*, 1994; *Abel and Thorne*, 1998a, 1998b] and controls the gradual decay of energetic outer belt electrons during quiet times [*Meredith et al.*, 2007; *Summers et al.*, 2007; *Lam et al.*, 2007]. In addition, PH is often observed in plumes, which could play a further role in shaping outer radiation belt dynamics [*Summers et al.*, 2008].

[5] Despite its recognized importance, the origin of PH has remained a hotly debated topic since its discovery [e.g., *Green et al.*, 2005, 2006; *Thorne et al.*, 2006; *Meredith et al.*, 2006]. Early theories proposed that ambient noise (i.e., the plasma thermal emissivity) would be amplified by freshly injected, hot, anisotropic electrons from the plasma sheet (~10–50 keV) to observable levels [*Thorne et al.*, 1973] in the outer region of the plasmasphere where the hot electrons overlapped the cool plasmasphere. Furthermore, the waves excited in this region would "recirculate" within the plasmasphere and return to the excitation region to be reamplified multiple times [*Thorne et al.*, 1979]. However, further study [*Huang and Goertz*, 1983; *Huang et al.*, 1983] showed that the total amplification was far too small to account for the observed PH amplitudes, leading *Church and Thorne* [1983] to conclude that the hot plasma could not, by itself, amplify the background waves sufficiently, and that some weak "embryonic source" of waves was necessary for further amplification. The first suggestion for what such an embryonic source could be, was given by *Church and Thorne* [1983, p. 7954] as "Chorus emissions that are highly unstable outside the plasmapause may enter the plasmasphere at high latitudes on trajectories in reverse to those of escaping plasmaspheric hiss." This suggestion was reiterated in later work [e.g., *Parrot et al.*, 2004; *Chum and Santolik*, 2005; *Santolik et al.*, 2006] although in these studies both the plasmapause and the effects of Landau damping were omitted from the model, which are indispensable elements in creating the observed characteristics of plasmaspheric hiss, as we discuss in the present work.

[6] Many other suggestions for the origin of PH have been advanced in the past 40 years, which have generally been dismissed due to theoretical issues or observational discrepancies. These include anthropogenic sources [*Molchanov et al.*, 1991; *Parrot et al.*, 1991], a "long-term" cyclotron instability due to electrons [e.g., *Etcheto et al.*, 1973; *Sazhin*, 1984, 1989] or protons [*Parady*, 1974], an ionospheric source due to unstable electrons [*Kovner et al.*, 1978] or protons [*Bud'ko*, 1984], as well as a "nonlinear" instability [*Storey et al.*, 1991]. A particularly interesting mechanism for the origin of PH involves the propagation and gradual evolution of lightning-generated, magnetospherically reflected whistlers into the incoherent hiss band [*Sonwalkar and Inan*, 1989; *Draganov et al.*, 1992, 1993], which can reproduce many of the observed features of PH [*Bortnik et al.*, 2003]. In fact, a statistical survey of satellite-observed wave power above 3 kHz showed a correlation with landmass which is consistent with the lightning origin of PH [*Green et al.*, 2005], but this study has led to some controversy [*Thorne et al.*, 2006; *Green et al.*, 2006] since the bulk of the PH power is found below 2 kHz (and more often, below 1 kHz). In an extensive follow-up study, *Meredith et al.* [2006] showed that the wave power above 2 kHz did indeed correlate well with landmass and quite probably had its source in terrestrial lightning strokes (thus confirming the results of *Green et al.* [2005]), but the power below 2 kHz had no such correlation, and in fact exhibited different properties to the power above 2 kHz, strongly suggesting that it had a different origin. There are a number of other issues concerning lightning as the origin of hiss, which are discussed in greater detail by *Bortnik et al.* [2009b, section 5].

[7] More recently, *Bortnik et al.* [2008] showed that the statistical properties of PH could be explained by considering whistler mode chorus (Figure 1b) as the origin of hiss.

By combining ray tracing in a realistic magnetospheric model, with Landau damping calculations using a measured distribution of suprathermal fluxes, it was shown that a certain fraction of chorus rays could propagate from their source region outside the plasmasphere into the plasmasphere and merge to form an incoherent PH spectrum having the correct bandwidth (~0.1–2 kHz), distribution in L shell, day-night asymmetry in power, dependence on geomagnetic activity (since chorus is geomagnetically controlled [*Meredith et al.*, 2001]), and other various ancillary features such as exohiss and ELF hiss. A fortuitous observation reported by *Bortnik et al.* [2009a] captured a one-to-one correlation of chorus and hiss in a specific event, having the appropriate time lag which was consistent with the proposed model. In the present paper, we extend and refine the analysis of *Bortnik et al.* [2008]. In section 2 we provide a detailed description of our cold plasma density model, and a substantially expanded and refined suprathermal electron flux model which we obtained from THEMIS observations. In section 3 we discuss the characteristics of a single chorus ray that has entered the plasmasphere, and in section 4 we show the distribution of lifetimes of the various rays as a function of initial L and wave normal angle. In section 5 we analyze a single-ray packet in detail with particular emphasis on the different morphologies of the rays, and summarize our main findings in section 6.

2. Model Description

[8] In order to study the propagation and evolution of chorus waves into plasmaspheric hiss, we use the HOTRAY code [*Horne*, 1989] to follow the trajectories of a large group of rays from their source region in the plasma trough, and calculate the path-integrated Landau damping of each ray. To do so, we need to make a number of assumptions concerning (1) the distribution and characteristics of the chorus source region, (2) the medium through which the rays propagate (i.e., the distribution of plasma density and the magnetic field model), and (3) the population of particles responsible for Landau damping (i.e., the distribution of suprathermal, 0.1–10 keV, electrons). Each of these factors is discussed in turn below.

2.1. The Chorus Source Region

[9] Chorus waves typically occur as a series of short (~0.1 s), coherent bursts of wave power that are confined to two frequency bands [*Burtis and Helliwell*, 1969] that scale with the equatorial gyrofrequency f_{ce}^{eq}: the lower band ($f/f_{ce}^{eq} \sim 0.1$–0.5, with a peak at $f \sim 0.34\ f_{ce}^{eq}$), and the upper band ($f/f_{ce}^{eq} \sim 0.5$–0.7, with a peak at $f \sim 0.53\ f_{ce}^{eq}$) [e.g., *Burtis and Helliwell*, 1976]. An example of a typical series of chorus elements observed on the THEMIS spacecraft [*Angelopoulos*, 2008] is shown in Figure 1b. Individual chorus elements are usually narrowband, meaning that each chorus element consists of a central frequency that varies with time ($df/dt \neq 0$), and a small bandwidth centered on this central frequency on the order of ~10 Hz [e.g., *Santolik et al.*, 2003]. The central frequencies of chorus elements are predominantly found to be rising ($df/dt > 0$, occurrence probability $P \sim 77\%$) at ~0.2–2 kHz/s (which increases with K_p and decreases with L shell), although they can also be falling ($df/dt < 0$, $P \sim 16\%$), or a combination of the above ($P \sim 18\%$) [*Burtis and Helliwell*, 1976]. Occasionally chorus emissions can also be more wideband and structureless [*Tsurutani and Smith*, 1974].

[10] The source region of chorus waves has been shown to lie in the low-density plasma trough [e.g., *Meredith et al.*, 2003; *Li et al.*, 2009], with wave power extending all the way from the plasmapause to $L \sim 10$ or higher [*Li et al.*, 2009]. Chorus waves show MLT dependence, and usually occur in the night, dawn, and day sectors [*Meredith et al.*, 2001, 2003; *Li et al.*, 2009]. Directional studies have shown that chorus usually propagates away from the equator, implying that the generation region is found at the equator [*LeDocq et al.*, 1998; *Lauben et al.*, 1998, 2002; *Santolik et al.*, 2005]. These observations have also been confirmed by numerical simulations that show the development of coherent chorus emissions in near equatorial regions [e.g., *Katoh and Omura*, 2007; *Omura et al.*, 2008]. However, we note that the precise details of the nonlinear triggering, growth, and saturation process are at present not well understood and remain a topic of intense research [e.g., *Nunn*, 1971; 1974; *Nunn et al.*, 2009; *Trakhtengerts et al.*, 1996, 2004; *Shklyar and Matsumoto*, 2009; *Bespalov et al.*, 2010; *Lampe et al.*, 2010; *Omura et al.*, 2008, 2009; *Schriver et al.*, 2010; *Santolik et al.*, 2010]. Studies of the wave normal distribution of chorus near the source region indicate that wave normals can take on a range of values, from predominantly field aligned [*Burton and Holzer*, 1974; *Goldstein and Tsurutani*, 1984; *Hayakawa et al.*, 1984; *Santolik et al.*, 2003] to ring-like [*Santolik et al.*, 2009] and oblique [*Lefeuvre and Helliwell*, 1985; *Hayakawa et al.*, 1990; *Lauben et al.*, 2002; *Tsurutani et al.*, 2008]. From a theoretical viewpoint, it is well known that a "small" radiating structure in a plasma will radiate waves over a broad range of wave normal angles [e.g., *Stenzel*, 1976] since a true plane wave would require either an infinitely large source region, or for the source region to be infinitely far away from the observer. Since it is known that the chorus transverse scales are small [e.g., *Santolik and Gurnett*, 2003; *Santolik et al.*, 2004], and the source region is equatorial, neither of these conditions can be true, and some finite radiation pattern must inevitably exist.

[11] For the purposes of our present modeling, we do not use the property that chorus is coherent and bursty, since we do not keep track of the coherence or temporal evolution of individual chorus elements, but only map wave power from one region of space to another. However, we use several other properties that are required of the source wave, including the excitation of the wave outside the plasmapause, the day/night symmetry specific to chorus, its relation to f_{ce}^{eq} and specifically the occurrence in two frequency bands that straddle $0.5\ f_{ce}^{eq}$, its dependence on geomagnetic activity, propagation away from the equator, source wave normal characteristics and distribution, and small spatial scales in the cross-B direction. We feel that no other emission but chorus fits this profile.

[12] To model the chorus source region to be consistent with the characteristics described above, we launch rays over a range of L shells from the outer edge of the plasmapause at $L = 4.8$, to $L = 7.6$ (where rays can no longer access the plasmasphere), in the lower-frequency portion of the chorus lower band ($f/f_{ce}^{eq} = 0.1$–0.3). At each equatorial injection point, and for each wave frequency, we

launch rays with a range of wave normal angles, from $-\psi_{res}$ to $+\psi_{res}$, where negative angles indicate wave normals pointing toward the Earth, and ψ_{res} is the resonance cone angle, beyond which propagation is not possible in a cold plasma.

[13] In addition, we restrict our ray tracing to the meridional plane (i.e., 2-D) which is computationally more efficient than the full 3-D ray tracing, yet still captures the key physical processes involved in the chorus propagation and evolution into PH. This assumption is consistent with observations that show chorus to be narrowly confined to its meridian [e.g., *Burton and Holzer*, 1974], in regions that do not have appreciable azimuthal gradients such as the night through to the morning sectors. However, on the dayside, and particularly during active conditions, large azimuthal gradients in number density are known to occur (e.g., formation of the plasmaspheric drainage plume), which result in significant azimuthal propagation, and thus the full 3-D propagation paths must be considered [*Chen et al.*, 2009].

2.2. The Propagation Medium

[14] We assume that the magnetic field of the Earth is dipolar and axially symmetric (with $f_{ce}^{eq}(R=1\,R_e)=870$ kHz), and that the plasma can be divided into two populations following *Kennel* [1966]: (1) a dense, cold component that predominantly controls the ray propagation and does not resonantly interact with the wave (i.e., $v_{thermal} \ll v_{ph}$) and (2) a hot, tenuous component responsible for the growth or damping of the ray (i.e., $\langle v \rangle \sim v_{ph}$). The advantage of this approach is that computation of the ray's refractive index n [e.g., *Stix*, 1992] and convective damping rate is considerably simpler when the plasma is assumed to be cold, than when it is "hot" and the full dispersion relation needs to be used [e.g., *Ichimaru*, 1973, p. 51; *Horne*, 1989], and thus ray tracing becomes appreciably faster. In addition, the form of the distribution of the suprathermal "hot" population does not need to be Maxwellian (or Kappa type distribution [e.g., *Summers and Thorne*, 1991]), but can be specified in a much more flexible way. The disadvantage of this approach is that cold plasma theory neglects a number of modes that would otherwise be present in a warm or hot plasma, especially when n becomes very large, near the resonance cone. We address this shortcoming by limiting n to a value that does not exceed a certain threshold, as discussed in section 5.2.

[15] The cold plasma model is a hybrid between the diffusive equilibrium model [*Angerami and Thomas*, 1964] and a superposition of an arbitrary number of field-aligned density structures (i.e., single- or double-sided ducts) that can produce a variety of realistic density distributions. The total density is specified as the product of a number of terms, as follows:

$$N_e = N_b N_{de} N_{li} N_{pl} \prod_{j=1}^{k} N_d^j \tag{1}$$

[16] Here, the multiplier N_b is the reference density value at the point R_b, which is measured from the center of the Earth. The second term N_{de} represents the diffusive equilibrium model [*Angerami and Thomas*, 1964] given by [e.g., *Kimura*, 1966; *Inan and Bell*, 1977]

$$N_{de} = \left[\sum_{i=1}^{3} \eta_i \exp(-G/H_i)\right]^{\frac{1}{2}} \tag{2}$$

where the subscripts $i = 1-3$ denote the ion species H^+, He^+ and O^+, respectively. η_i is the ion composition at $R = R_b$, G is the geopotential height

$$G = R_b(1 - R_b/R)$$

and H_i is the scale height for each ion species

$$H_i = \frac{k_B T_{DE}}{M_i m_p g(R_b)}$$

where

$$g(R_b) = g(R = R_E)\left(\frac{R_E}{R_b}\right)^2$$

and M_i is the ion mass normalized by the proton mass, m_p, T_{DE} is the temperature at the base of the diffusive equilibrium model, and k_B is the Boltzmann constant.

[17] The lower ionosphere term, N_{li}, is used to reduce the density below the ionosphere to zero and to create a peak representing the ionosphere. It is specified as

$$N_{li} = \begin{cases} 1 - \exp\left(-\frac{(R-R_0)^2}{H^2}\right) & \text{if } R \geq R_0, \\ 0 & \text{otherwise} \end{cases} \tag{3}$$

where R_0 is the geocentric distance to the bottom of the ionosphere where the density goes to zero and H is the scale height of the bottomside of the lower ionosphere.

[18] The plasmapause term, N_{pl}, creates the sharp density gradient at the plasmapause, and is specified as

$$N_{pl} = \begin{cases} \exp\left(-\frac{(L-Lp)^2}{w^2}\right) + \left(1 - \exp\left(-\frac{(L-Lp)^2}{w^2}\right)\right) \times \ldots \\ \quad \left(\left(\frac{R_c}{R}\right)^a + \left(1 - \left(\frac{R_c}{R}\right)^a\right) \exp\left(-\frac{(R-R_c)^2}{H_s^2}\right)\right) & \text{if } L \geq L_p, \\ 1 & \text{otherwise} \end{cases} \tag{4}$$

where L_p is the L shell at the inner edge of the plasmapause, w is the half width of the plasmapause boundary (in units of L), R_c is the geocentric distance to the level at which the density outside the plasmapause field line is equal to the density inside, a determines how the density falls off outside the plasmapause and H_s is the scale height of the radial density decrease for $R \geq R_c$ and outside the plasmapause.

[19] The duct terms N_d, are used to adjust the equatorial density profile to any desired distribution, and any arbitrary number of ducts k, may be included. Using these ducts to adjust the equatorial distribution has the advantage that off-equatorial regions are automatically adjusted in a smooth, continuous, and physical way. Each duct is specified as follows:

$$N_d = 1 + d_d f_f f_r \tag{5}$$

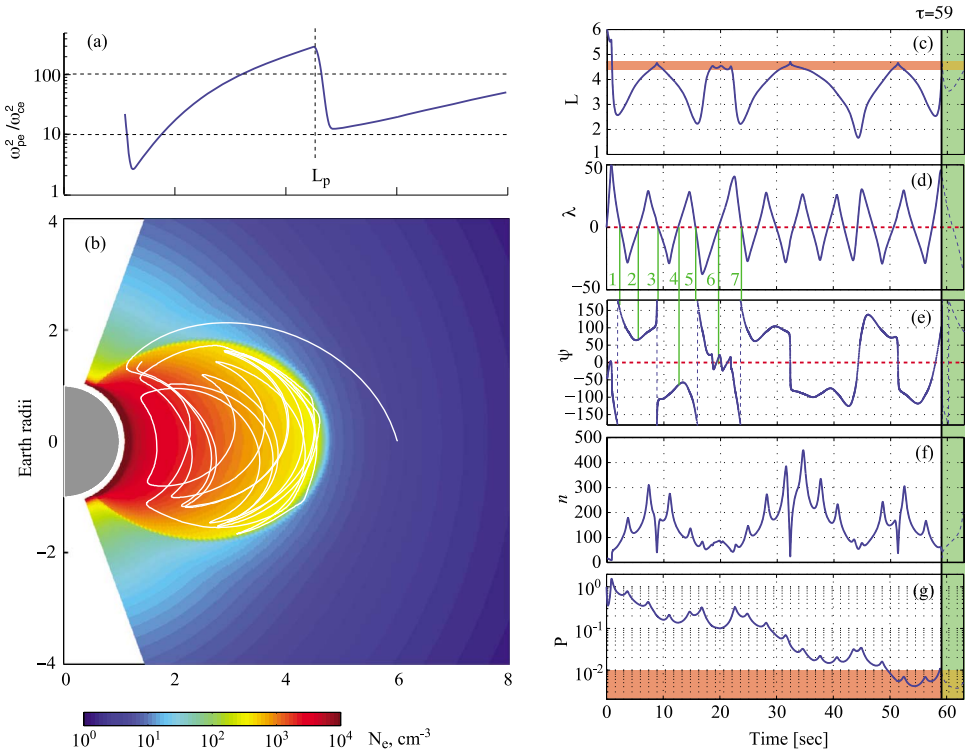

Figure 2. An example of a typical chorus ray that has entered the plasmasphere and evolved into plasmaspheric hiss. (a) Plasma parameter distribution along the equatorial plane, $\omega_{pe}^2/\omega_{ce}^2$, where the dashed lines indicate typical values of 10–100; (b) raypath in a meridional plane at MLT = 10; (c) local L shell of the ray; (d) local ray latitude λ; (e) wave normal angle relative to the local magnetic field direction ψ; (f) refractive index n; and (g) relative wave power P.

where d_d is the duct enhancement factor (i.e., fractional increase above the ambient density), and

$$f_l = \begin{cases} \exp\left(-\frac{(L-L_d)^2}{W_d^2}\right) & \text{if } L > L_d, \\ 1 & \text{otherwise} \end{cases}$$

and

$$f_r = \begin{cases} \exp\left(-\frac{(R-R_u)^2}{W_u^2}\right) & \text{if } R < R_u, \\ 1 & \text{otherwise} \end{cases}$$

[20] The term f_l indicates that we are using a one-sided duct, and is used to roll off the density as a function of L beyond the duct center, L_d, with a width of W_d. The term f_r controls how the duct density varies along the field line, up to the geocentric radius R_u, with a width W_u.

[21] The parameter values corresponding to the dayside used in the rest of this paper are: $R_E = 6370$ km, $g(R = R_E) = 9.81$ ms^{-2}. $R_0 - R_E = 90$ km, $H = 140$ km, $T_{de} = 1600$ K, $R_b - R_E = 1000$ km, $N_b = 3.1 \times 10^9$ m^{-3}, $\eta_1 = 8\%$, $\eta_2 = 2\%$, $\eta_3 = 90\%$, $L_p = 4.5$, $w = 0.13$, $a = 2$, $R_c = 5500$ km, $H_s = 500$ km, $k = 2$, i.e., two identical ducts are added with the following parameters: $d_d = 1.8$, $L_d = 1.1$, $W_d = 2.55$, $R_u = 4000$ km, $W_u = 20000$ km. The nightside values are identical except for the following parameters: $w = 0.10$, $R_c = 4000$ km, $H_s = 4000$ km. A plot of the plasma frequency normalized by the gyrofrequency and electron number density in the meridional plane is given in Figures 2a and 2b, respectively, using the above model and dayside parameters. These parameter values were chosen to fit the equatorial number density to the model of *Carpenter and Anderson* [1992], under typical day and night conditions. The diffusive equilibrium model, on its own, cannot produce this equatorial profile, and thus we have chosen to include two additional, one-sided ducts. We also constructed our model to ensure that the field-aligned distribution is as realistic as possible. For example, fitting the commonly used function $n_e = n_{e0}$ (cos $\lambda)^{-2\alpha}$ to our model, we obtain $\alpha \sim 2.7$ at $L = 6$, which is consistent with observed values (e.g., *Denton et al.* [2006] gets $\alpha = 2.6$ for $L = 5$–6, and $\alpha = 2.8$ for $L = 6$–7).

[22] We have placed the inner edge of the plasmapause at $L_p = 4.5$ to model moderately disturbed conditions, such as may be experienced in the recovery phase of a geomagnetic storm (e.g., corresponding to $K_p \sim 2.4$ [after *Carpenter and Anderson*, 1992]). We have chosen to model a less disturbed period than *Bortnik et al.* [2008] because, even though chorus intensities increase with increasing geomagnetic activity, the probability of occurrence of chorus maximizes for moderate wave amplitudes (which, on average, correspond to moderately disturbed conditions), occasionally reaching ~40% for waves in the range $10 < B_w < 30$ pT [*Li et al.*, 2009]. To model the most probable situation, we have thus chosen to concentrate on moderately disturbed periods.

2.3. The Suprathermal Electron Flux Model

[23] The distribution of suprathermal electron fluxes is critical in determining the extent of Landau damping that each ray experiences, and thus the number of rays that leak into the plasmasphere, their power, and ultimately the PH frequency spectrum all as a function of MLT. To obtain the most accurate model, we used THEMIS data [*Angelopoulos*, 2008] collected over the period 1 June 2008 to 1 February 2010. The THEMIS probes are ideally situated to perform this measurement due to their near-equatorial orbits (within ~20° of the equator), broad coverage in L with apogees extending above 10 R_E and perigees below 2 R_E, and full coverage in MLT. The THEMIS suprathermal electron data set is a significant improvement to the CRRES data set used by *Bortnik et al.* [2007a, 2007b, 2008], since it avoids the MLT coverage gap in the afternoon sector, and also does not saturate inside the plasmasphere, allowing us to use measured fluxes as opposed to the model of *Bell et al.* [2002] as was done previously. This latter point is important because the model of *Bell et al.* [2002] was found to hold only deep inside the plasmasphere, whereas closer to the plasmapause the suprathermal fluxes tend to increase rapidly [see *Li et al.*, 2010, Figure 4], which has implications for the Landau damping of obliquely propagating rays that approach the inner edge of the plasmapause. A full discussion of the analysis method is provided by *Li et al.* [2010] and is summarized below for convenience.

[24] We use data from the electrostatic analyzer (ESA) which provides electron distributions from a few eV to 30 keV [*McFadden et al.*, 2008]. ESA data from THEMIS probes A, D, and E is collected, and radiation belt contamination is then removed. The data is then sorted according to its location, either inside the plasmasphere or outside of it, which is determined by using the spacecraft potential as a proxy for the cold electron number density. The data is then binned into 0.5 L × 1 MLT bins, and further separated by the level of geomagnetic activity. The flux distributions used in the present paper are shown by *Li et al.* [2010, Figures 3 and 4]. We have used the middle column corresponding to $100 < AE^* < 300$ nT, for consistency with our assumption of moderately disturbed conditions.

[25] Using 5 energy channels in the range 0.1–10 keV (namely 108, 324, 975, 2927, and 8788 eV), a function of the form $f(v) = A/v^n$ is fitted to each L-MLT bin similar to *Bortnik et al.* [2007a] and is then used to calculate the local Landau damping rates using the formalism given by *Kennel* [1966] (later rewritten by *Brinca* [1972], whose work was used by *Bortnik et al.* [2007a, 2007b, 2008]). This particular energy range was chosen based on the typical Landau resonant energies of our chorus rays, which are usually ~1 keV and rarely exceed a few keV.

3. Single-Ray Example

[26] We illustrate a few typical features of chorus ray propagation using the single-ray example shown in Figure 2. Here we plot a ray launched at $L = 6$, $\lambda = 0°$, with $f = 0.1\, f_{ce}^{eq} \sim 403$ Hz, and initial wave normal angle $\psi_0 = -45°$. The ray is allowed to propagate until its power reaches 1% of its initial value, at which point the ray is terminated and the time at which this occurs is called the ray lifetime τ. The suprathermal electron distribution corresponding to MLT = 10 is used (both inside and outside the plasmasphere) to represent dayside conditions.

[27] Figure 2b shows the ray trajectory in the meridional plane and illustrates the point that even though only a single ray was traced, representing only a single frequency, L shell, and ψ_0, it is nevertheless able to fill virtually the entire plasmasphere during its lifetime. Comparing Figures 2c and 2d, the ray enters the plasmasphere at $t = 0.85$ s at a high latitude ($\lambda = 51°$), and performs a sequence of excursions to low L shells where it undergoes magnetospheric reflections (that is, ψ rotates through 90°), followed by excursions to high L shells where it undergoes reflections from the plasmapause (that is, ψ rotates through 0° or 180°), highlighted with the brown bar in Figure 2c. There are, of course, deviations from this typical cyclical trajectory for some rays where magnetospheric reflections occur at high L shells (e.g., at $t = 35$ s, $L \sim 4.2$).

[28] An interesting consequence of the cyclical trajectory performed by the ray is that the wave normal angle during equatorial crossings tends to become nearly field aligned, and hence the severe Landau damping that is usually present near the equator is largely avoided. This is illustrated by comparing Figures 2d and 2e, where we have marked the first 7 equatorial crossings with green vertical lines, showing that for 5 of the 7 crossings the wave normal angle is exactly field aligned, and the remaining 2 crossings have angles in the range ~50°–70°. Furthermore, the 5 equatorial crossings correspond to either a low-L excursion (crossings 1, 5 and 7), or plasmapause reflections (crossings 3 and 6). Figure 2e shows that plasmapause reflections typically involve a strong rotation of the wave normal in the negative direction (i.e., anticlockwise in our geometry or in the direction back into the plasmasphere), which tends to "pull" ψ toward the field-aligned orientation, reducing damping, and maintaining the ray's cyclical trajectory. This underscores the importance of plasmapause reflections in the process of extending the ray lifetime and thus sustaining the hiss emission. Figure 2f shows the value of the refractive index n during the course of propagation, and a comparison of Figures 2f and 2d reveals that the local maxima in n are associated with magnetospheric reflections of the ray, i.e., rotation of ψ through 90°.

[29] Figure 2g shows the evolution of the ray's relative power, by which we mean the total integrated wave gain (where only the $m = 0$ or Landau resonance is included), multiplied by the geometric contraction factor $G = r_0 \cos(\lambda_0)/r\cos(\lambda)$, to account for the azimuthal convergence of magnetic field lines at high latitudes and smaller geocentric distances. In this context, we note that we have made no attempt to keep track of the geometric contraction factor associated with meridional propagation, even though the wave energy density will inevitably increase due to the smaller volume associated with lower L shells. The reason for this, is because rays that propagate within a single meridian do not conform to their specific L shells (unlike rays in adjacent meridians that remain cleanly separated in a cylindrically symmetric model), but can cross L shells, converge, diverge, and reflect multiple times, so there is no single meridional geometric contraction factor that can be defined. Instead, a fundamentally different approach is required that defines an observation location at some given location in space, and essentially counts individual rays that

cross this location, thus losing track of individual ray identities [see, e.g., *Bortnik et al.*, 2003]. In the present study, we keep track of individual ray identities and examine their evolution, leaving the study of the full wave distribution to future work.

[30] We have also not taken into account first-order cyclotron growth, because linear growth calculations based on measured distributions often result in unrealistically large integrated gains of over 100 dB [*Li et al.*, 2008], and a proper treatment requires the inclusion of nonlinear effects to saturate the wave at reasonable amplitudes, which is beyond the scope of the present study. Instead, we assume that the chorus wave are instantaneously switched on at the equator as in previous studies [e.g., *Bortnik et al.*, 2007a, 2007b, 2008], as an approximation to the small growth region of chorus waves near the equator.

[31] Since only Landau damping has been included, the peaks that occur periodically in Figure 2g are attributed to the azimuthal contraction factor; that is, they are associated with either the ray's inward motion (i.e., reduction in r) or its propagation to high latitudes (i.e., increase in λ). We note that the lifetime τ is taken at the last time that the ray's power crosses the 1% threshold, so that reversible fluctuations in power (i.e., due to geometric contraction) do not cause the ray to be eliminated prematurely. This threshold is shown with the brown block in Figure 2e, and the final lifetime is marked with the green block, giving $\tau = 59$ s.

4. Distribution of Ray Lifetimes

[32] We now repeat the ray tracing process discussed above, but scan over a range of initial wave normal angles ψ_0, initial L shells, wave frequencies, and MLT sectors to represent the chorus source region as described in section 2.1. For each set of initial parameters, we perform the ray tracing, compute the path-integrated Landau damping, and record the lifetime τ. The results of this simulation are shown in Figure 3b as a lifetime "map" plotted as a function of ψ_0 and L_0, parameterized by wave frequency $f/f_{ce} = 0.1$, 0.2, and 0.3 in the top, middle, and bottom rows, respectively, and MLT = 0, 6, and 10, in the left, middle, and right columns, respectively. The suprathermal electron fluxes for the appropriate MLT sectors are selected in the simulation, and the cold plasma density is chosen to be the dayside model for MLT = 10 and 6, and the nightside model for MLT = 0.

[33] As an additional constraint on lifetimes, we limit the magnitude of the refractive index to values that are relatively small (i.e., such that the wave's phase velocity is much larger than the plasma thermal velocity), so as to preserve the integrity of the cold plasma assumption. An approximate expression of this value was given by *Boskova et al.* [1988, equation 3] as

$$n_{\max}^2 \sim \frac{c}{v_{\text{th}}} \frac{\omega_{\text{pe}}\omega_{\text{ce}}}{\omega^2} \tag{6}$$

where v_{th} is the thermal velocity of the plasma, and for a 1 eV plasma, $c/v_{\text{th}} \sim 500$. For the range of $\omega_{\text{pe}}/\omega_{\text{ce}}$ values shown in Figure 2a, and typical wave frequencies used in our simulation, $n_{\max} \sim 500$–2000. This constraint affects a 1small fraction of the rays that have entered into the plasmasphere, have settled into a pattern of magnetospheric reflections, and slowly drift toward their LHR surface while becoming progressively more oblique and electrostatic. At the point where the phase velocity of the wave starts to approach the thermal velocity of the plasma, the cold plasma approximation becomes progressively less accurate, and requires higher-order correction terms in the dispersion equation [e.g., *Swanson*, 1989, equation 3.37, pp. 82–88; *Stringer*, 1963; *Sazhin*, 2005]. One consequence of this is that the refractive index surface becomes closed at $\psi \sim 90°$ above the lower hybrid resonance frequency, by the introduction of thermal wave modes, and $\mathbf{k} \cdot \mathbf{v_g}$ can take large values leading to rapid Landau damping (here, $\mathbf{v_g} \equiv \partial\omega/\partial\mathbf{k}$ is the group velocity). We have used $n_{\max} = 500$ for the results shown in Figure 3, but the precise value of $n_{\max}$ is not critical, because when n starts to become large (i.e., $n > 500$) in the course of successive magnetospheric reflections near the LHR surface, it quickly grows to values of several thousand. For comparison, we have reproduced Figure 3 using $n_{\max} = 1000$ and $n_{\max} = 2000$ (not shown), and the results are indistinguishable from the current Figure 3, confirming that the exact value of $n_{\max}$ is not critical, as long as n is clamped at some reasonably large value that prevents it from propagating indefinitely.

[34] Figure 3b shows that in every panel, there is region in the ψ_0 - L_0 plane with $\tau > 10$ s (i.e., with color in the orange-red range), which corresponds to those rays that have entered the plasmasphere and perform long-lived cyclical trajectories (referred to as "hiss rays" below). Rays with $\tau < 1$ s are typically damped before reaching the plasmasphere, and rays with $1 < \tau < 10$ s exhibit a range of intermediate morphologies, that are discussed further in section 5. Even though hiss rays are present in every panel, suggesting that chorus contributes to the plasmaspheric hiss power in every MLT sector, the region occupied by these rays in the ψ_0 - L_0 plane shows a systematic behavior, increasing with increasing MLT, and with decreasing f. This behavior reflects two different effects: the first is the dependence of the Landau damping rate on the ratio $r_n = n_h/n_0$, i.e., the number of hot (suprathermal) particles compared to the number of cold particles. On the nightside, suprathermal fluxes are large due to injection of plasma sheet particles, and progressively diminish as they drift through the dawnside to the dayside, due to scattering by waves. On the other hand, the cold plasmadensity is smallest at night, and increases with increasing MLT as the earth rotates to the sunlit side, and outflow from the ionosphere replenishes the plasma trough. The MLT trends in n_h and n_0 both contribute to creating a maximum r_n on the nightside, and a minimum on the dayside, resulting in weak damping and long lifetimes. The second factor which increases the hiss ray region in Figure 3b is dependence of resonant energies on f through the resonance condition [e.g., *Kennel and Petschek*, 1966], higher energies resonating with lower f. Since the flux of suprathermal electrons typically decreases with increasing energy, lower f resonates with a lower flux of particles, decreasing the damping rate and increasing τ.

[35] These trends are consistent with the statistical behavior of plasmaspheric hiss, which shows larger wave power on the dayside, compared to the nightside [*Meredith et al.*, 2004]. Since chorus wave power is known to be geomagnetically controlled [*Meredith et al.*, 2003; *Li et al.*,

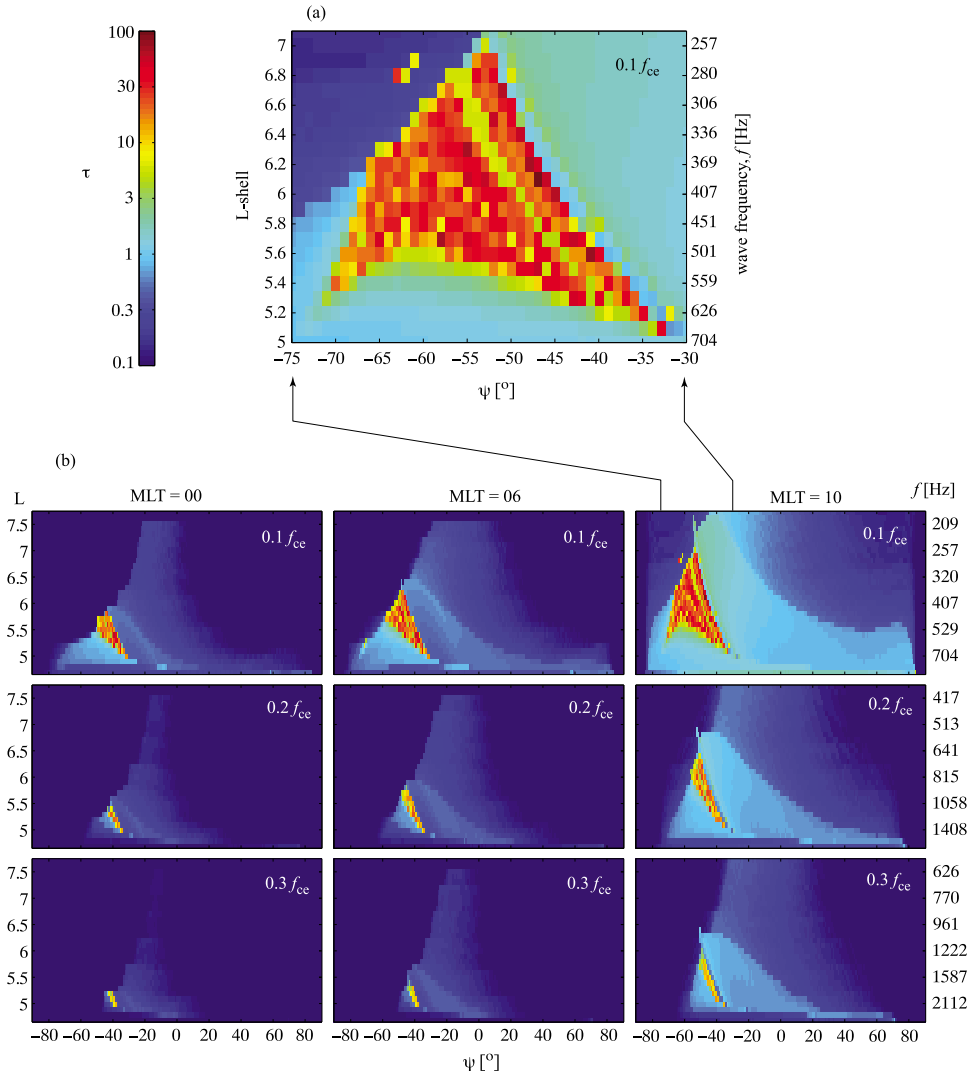

Figure 3. Lifetime of chorus rays (in seconds) launched with initial wave normal angle and L shell shown on the abscissa and ordinate, respectively. (a) Expanded lifetime map showing hiss rays and (b) lifetime maps, parameterized according to wave frequency (f/f_{ce}^{eq} = 0.1, 0.2, and 0.3 in the top, middle, and bottom rows, respectively) and MLT sector (MLT = 00, 06, and 10 in the left, middle, and right columns, respectively).

2009], the plasmaspheric hiss that arises from chorus, would thus naturally show the same dependence on geomagnetic activity, consistent with observation [*Meredith et al.*, 2004, 2006].

[36] The panel corresponding to the largest hiss ray region, and longest τ values (f = 0.1 f_{ce}, MLT = 10) is expanded and shown in Figure 3a. Here, the hiss region occupies ψ_0 = −32° to −71°, and L_0 = 5.1–6.9, although the bulk of the hiss rays originate from L > 5.5, indicating that there is a small region of L ~ 0.5–1 immediately outside the plasmapause where chorus rays cannot easily enter the plasmasphere, and turn into hiss rays. This is due to the specific conditions required to set up the cyclical trajectories within the plasmasphere, namely entry into the plasmasphere at high latitudes, roughly λ > 25°. The extent of the hiss ray region in L can be immediately converted to an absolute frequency scale (right-side ordinate in Figure 3a), showing that the bandwidth of the hiss rays lies in the range ~250–600 Hz for this particular chorus frequency component, consistent with observed values [*Thorne et al.*, 1973]. In order to obtain a more realistic representation of the entire hiss spectrum, contributions from other chorus frequency components need to be included (e.g., Figure 3b), which will add a component of progressively diminishing power up to ~2 kHz.

5. Ray Morphologies

[37] We now examine the variety of ray morphologies that make up a full distribution of ψ_0, for a typical starting location (L_0 = 6) and frequency f = 0.1 f_{ce}. The results are shown in Figure 4 and are organized by their lifetimes (Figure 4f) into four distinct classes of rays, shown in Figures 4b–4e. Figure 4a shows all the rays from the entire distribution spanning ψ_0 = −85° (dark blue) to +85° (dark red). Immediately evident is the entry of hiss rays into the

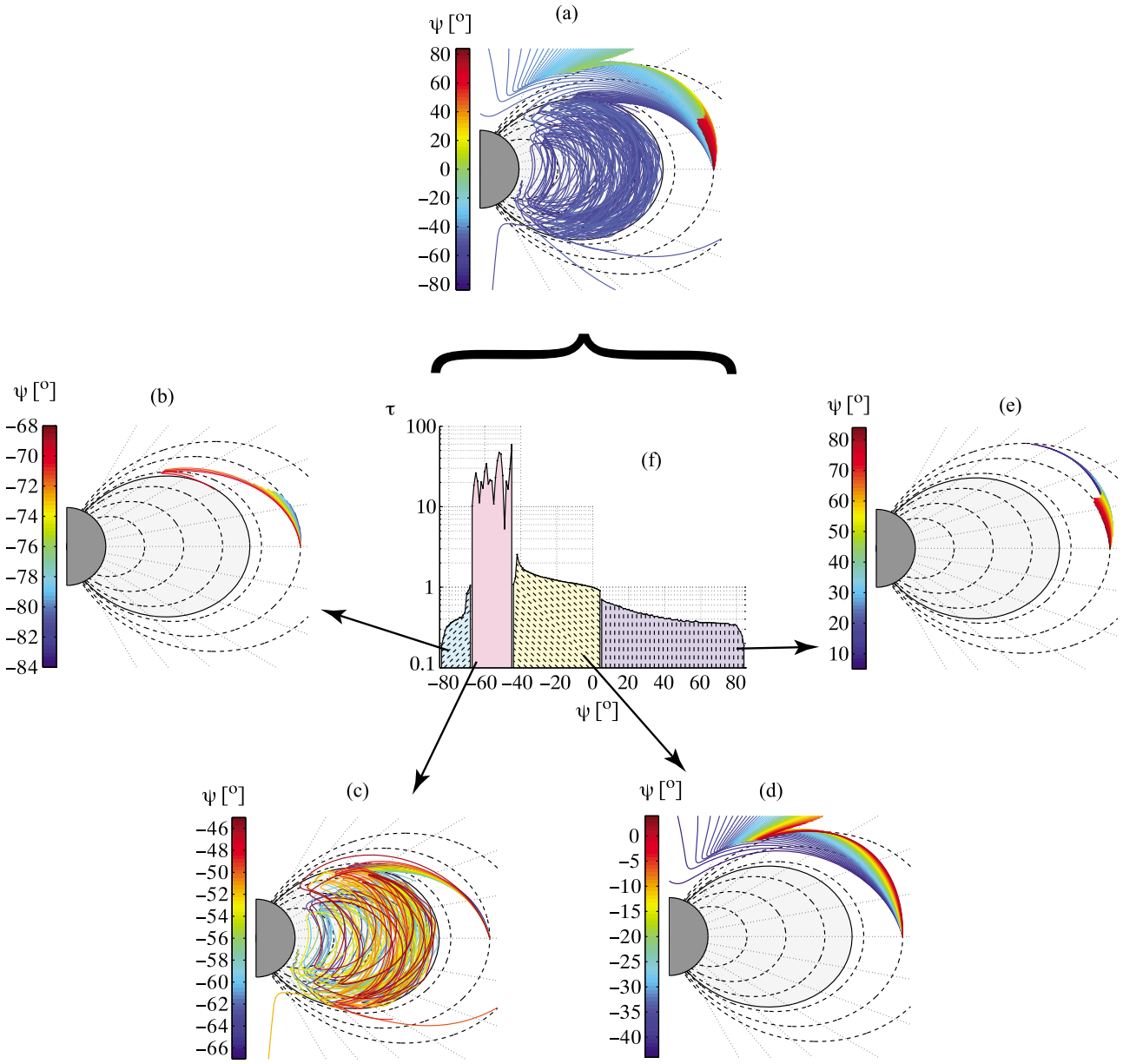

Figure 4. Morphology of chorus rays injected at L = 6 and MLT = 10 with 1° intervals in ψ_0. (a) All raypaths in the range ψ_0 = −85° to +85°; (b) group 1 rays, ψ_0 = −85° to −68°; (c) group 2 "plasmaspheric hiss rays," ψ_0 = −67° to −45°; (d) group 3 "ELF hiss rays," ψ_0 = −44° to +4°; (e) group 4 "quasi-parallel rays," ψ_0 = +5° to +85°; and (f) ray lifetimes as a function of ψ_0 for the four groups, in seconds.

plasmasphere at high latitudes, and the dense filling of the plasmasphere with rays starting from L = 1.5 and extending all the way to the plasmapause. There are also some rays that are trapped in the ionospheric LHR duct, some that traverse the plasmasphere and emerge once again into the plasma trough, some that magnetospherically reflect and propagate to higher L shells, and some that are damped on their first hop. Each of these rays are discussed below.

5.1. Group 1: ψ_0 = −85° to −68°

[38] The first group of rays (Figure 4b) shows a monotonic rise in lifetimes from τ (ψ_0 = −85°) ~ 0 s to τ (ψ_0 = −68°) ~ 1 s. The propagation paths grow accordingly, such that the majority of rays are damped at midlatitudes, λ_f = 10°–20°. There is a sharp transition in behavior between ψ_0 = −71° and ψ_0 = −70°, the former ray being damped during its first hop to higher latitudes, within ~0.5 s, and reaching λ_f m 19°, whereas the latter ray propagates to λ = 38°, undergoes a magnetospheric reflection (MR), and propagates back to lower latitudes while being guided by the plasmapause density gradient. These MR rays are not the usual type that are generated by lightning [*Bortnik et al.*, 2003], in that their wave normal points inward, toward lower L, as opposed to outward. If our density model was uniform, these rays would propagate to lower L, but in the present case, the plasmapause guides the ray, which could

result in an accumulation of whistler wave power near the plasmapause. Since the wave normal angle of these rays is highly oblique, rapid damping extinguishes the rays within a few degrees of their MR point.

5.2. Group 2: Hiss Rays, $\psi_0 = -67°$ to $-45°$

[39] The second group of rays (Figure 4c) corresponds to the "hiss rays" discussed in section 4 (red region in Figure 3a), spans the range $\psi_0 = -67°$ to $-45°$, and has lifetimes on the order of tens of seconds, which do not behave systematically with increasing ψ_0 (pink region in Figure 4f). The general morphology of hiss rays is discussed in section 3, and shown in Figure 2, and involves the propagation of chorus rays from their origin ($L_0 = 6$, $\lambda_0 = 0°$ in this example) to high latitudes where the rays enter into the plasmasphere, then propagate toward the equator, and perform a sequence of MRs and plasmapause reflections (PR). However, since the plasmaspheric entry point of each ray is slightly different, the cyclical ray orbits all start with slightly different initial conditions which causes the ray trajectories to diverge within the first few bounces, exhibit a variety of morphologies, and take on somewhat chaotic τ values.

[40] Comparing Figures 3a and 4f, a systematic minimum in τ is visible in Figure 3a extending from $\psi_0 = -37°$ at $L = 5.2$ diagonally upward to $\psi_0 = -57°$ at $L = 6.8$, which corresponds to the minimum hiss ray lifetime ($\tau = 5$ s) at $\psi_0 = -49°$ at $L = 6$ in Figure 4a. These rays all exhibit the same morphology, entering the plasmasphere at high latitude ($\lambda \sim 35°$), crossing the equator only once, and exiting the plasmasphere at high latitude ($\lambda \sim 40°$) in the opposite hemisphere. In order to attain the correct initial conditions (to perform only a single traverse) at the plasmaspheric entry point, rays injected at increasing values of L_0 must be initiated with increasingly negative values of ψ_0, as is evident in Figure 3a. Rays initiated in the range $\psi_0 = -51°$ to $-46°$ all eventually exit the plasmasphere after performing a number of cyclical trajectories, and may be the source of exohiss [*Thorne et al.*, 1973].

[41] It is interesting to observe that a number of rays are able to enter and propagate horizontally within the ionosphere prior to damping out, in this case rays with $\psi_0 = -63°$ and $-55°$. This effect is not particular to $L_0 = 6$, but is observed consistently over the range $L_0 \sim 5.5$–6.5, and possibly even more, if a finer resolution in ψ_0 is used. The rays propagate with high wave normal angles in a direction that is roughly perpendicular to the geomagnetic field, and are trapped between two horizontal layers that alternately refract the rays back into the ionosphere. In this sense, the rays are consistent with an effect that has been analyzed previously and called LHR duct trapping [*Smith et al.*, 1966; *Gross*, 1970], whose latitude-dependent signature has been observed on low-altitude spacecraft at frequencies below a few kHz [*Ondoh et al.*, 1982, 1983]. The possibility that the ionospheric hiss resulting form LHR duct trapping may be related to chorus is only mentioned here in passing, and the full analysis is left for future studies.

[42] As a final note, we mention the effect of restricting the refractive index to values below $n = 500$, to preserve the integrity of the cold plasma assumption. This affects the lifetimes of four hiss rays, with $\psi_0 = -57°$, $-56°$, $-54°$, and $-53°$. For comparison, if $n_{max} = 1000$ as opposed to $n_{max} = 500$, the lifetimes of the four rays above become 26.4, 35.3, 28.1, and 38.3 s, instead of 21.4, 20.8, 22.9, and 37 s, respectively. These rays all follow the same morphology and settle into a pattern of MR, where ψ become progressively more oblique as a function of time, and n tends to infinity (in the cold plasma approximation) concomitantly. After n becomes large ($n \sim 500$–1000), neither the ray tracing nor the damping calculation can be considered to be reliable, because the thermal modification to the refractive index affects the ray trajectory (slightly), and the damping calculation (substantially) through the value of n. In addition, since the wavelength becomes progressively smaller with increasing n, and falls below ~1 km for typical frequencies and $n > 500$, it is able to scatter off small-scale irregularities in the plasmasphere and be extinguished rapidly. An accurate treatment of these effects is well beyond the scope of the present work, and hence we choose to limit our rays to $n_{max} = 500$ where our current model is a good approximation to the full treatment.

5.3. Group 3: ELF Hiss Rays, $\psi_0 = -44°$ to $+4°$

[43] The third group of rays (Figure 4d) occupies the range $\psi_0 = -44°$ to $+4°$, and has the distinctive feature of propagating to high latitudes $\lambda > 45°$ and magnetospherically reflecting toward higher L shells. The lifetime values of group 3 rays are fairly uniform at $\tau \sim 1$ s, and most likely represents the ELF hiss emission, which is a hiss found at high latitudes, propagates away from the Earth, and has been shown to be correlated to discrete chorus emissions [*Santolik et al.*, 2006]. There is a sharp transition in morphology at the critical value $\psi_0 = \psi_{crit} \sim -45°$, with rays below ψ_{crit} propagating to lower L and evolving into PH, and rays above ψ_{crit} propagating to higher L and evolving into ELF hiss. This bifurcation in behaviors has been reported previously [*Thorne and Kennel*, 1967; *Chum and Santolik*, 2005; *Bortnik et al.*, 2007b]. It seems very likely that the chorus observed on the ground and low-altitude spacecraft is initiated with $\psi_0 \sim \psi_{crit}$, is able to avoid the region of rapid Landau damping at midlatitudes, and impinge on the ionosphere with roughly vertical wave normal angles, which have the largest probability of propagating through the ionosphere and to the ground.

5.4. Group 4: Typical Chorus, $\psi_0 = +5°$ to $+85°$

[44] The fourth and final group of rays (Figure 4e) occupies the range $\psi_0 = +5°$ to $+85°$, and becomes completely damped during its "first hop," i.e., propagation from its equatorial source region toward higher latitudes. Even though this morphology may be the least interesting of all the groups discussed above, it is nevertheless very important since it is generally believed that the majority of the chorus wave power is concentrated at low values of ψ_0. This stems from theoretical considerations that predict maximum growth rates at $\psi_0 \sim 0°$ [e.g., *Kennel*, 1966; *Kennel and Thorne*, 1967], as well as some satellite observations near the chorus source region [*Burton and Holzer*, 1974; *Goldstein and Tsurutani*, 1984; *Hayakawa et al.*, 1984; *Santolik et al.*, 2003]. The propagation characteristics of $\psi_0 \sim 0°$ rays are also the most consistent with the statistical spatial distribution of chorus wave power [*Bortnik et al.*, 2007a], underscoring that it is this group which predominantly represents the behavior of the bulk of the chorus

wave power. As expected, τ diminishes monotonically with increasing ψ_0, from τ (ψ_0 = +5°) ~ 0.7 s to τ (ψ_0 = +85°) ~ 0 s.

6. Discussion and Conclusions

[45] In the foregoing analysis, we presented the behavior of a population of chorus rays, distributed in L shell, and ψ_0, and parameterized according to MLT and f. This analysis is similar to the one presented by *Bortnik et al.* [2008, hereinafter B08] that first described the origin of plasmaspheric hiss as an evolution of chorus rays that have propagated into the plasmasphere at high latitudes, by avoiding Landau damping and performing a sequence of magnetospheric and plasmaspheric reflections inside the plasmasphere for tens of seconds. Compared to B08, however, we have significantly revised our models and input parameters in the present paper: here we use the HOTRAY ray tracer [*Horne*, 1989] which allows for either cold or hot plasma ray tracing, as opposed to the Stanford VLF ray tracer [*Inan and Bell*, 1977] discussed by B08 which only allows cold plasma ray tracing, we use an L-dependent, MLT-dependent suprathermal flux distribution to calculate Landau damping both inside and outside the plasmasphere, measured by the THEMIS satellite cluster [*Li et al.*, 2010] which has high sensitivity and complete coverage, as opposed to the study by B08,which used a single (L- and MLT-independent) suprathermal flux model inside the plasmasphere measured on the Polar satellite [*Bell et al.*, 2002] and an L- and MLT-dependent flux model outside the plasmasphere measured on the CRRES satellite which had good sensitivity but gaps in coverage [*Bortnik et al.*, 2007a]. We also modified our cold plasma model to reflect moderately disturbed conditions (L_p = 4.5) as opposed to the more disturbed plasma model parameters used by B08 (L_p = 3.6). Despite the extensive changes and improvements in our model and parameters, the basic conclusions remain essentially unchanged from those of B08 on the nightside, and very similar on the dayside where we have analyzed MLT = 06 and MLT = 10, as opposed to MLT = 15 found by B08 (due to the poor coverage of CRRES at lower MLT on the dayside).

[46] Our results show that the region of chorus rays in the L_0 - ψ_0 plane that can access the plasmasphere and become hiss rays increases with increasing MLT and exhibits longer lifetimes, consistent with the observationally well-known MLT asymmetry of hiss, which shows a maximum of wave power on the day and a minimum at night [*Meredith et al.*, 2004, 2006]. The hiss ray region also increases with decreasing wave frequency, which is well explained by the behavior of Landau damping (i.e., lower damping and hence longer lifetimes at lower frequencies).

[47] A detailed examination of the raypaths originating from L = 6 showed a division into four basic categories: (1) rays that were damped on their first hop from the equator to high latitudes, or that were trapped on the plasmapause boundary enduring for ~1 s or less; (2) rays that entered into the plasmasphere, and that evolve into plasmaspheric hiss, enduring for tens of seconds; (3) rays that magnetospherically reflect to higher L at high latitudes and most likely evolve into the ELF hiss emission, enduring for ~1 s; and (4) rays that are roughly field aligned, carry the bulk of the chorus wave power, and are damped at midlatitudes within 1 s. Each of these categories of rays behaves morphologically differently, and in most cases corresponds to distinct emissions that have been observed in the inner magnetosphere. Interestingly, we showed that within category 2 rays, a subset of rays was able to enter and propagate horizontally within the ionosphere, which may be related to a previously reported phenomenon called LHR ducting.

[48] **Acknowledgments.** The authors would like to acknowledge the NSF for their support of this work through grant AGS-0840178, the AFRL through grant FA9550-08-1-0140, and the THEMIS team for their distribution of an outstanding data set without which this work would not have been possible.

[49] Robert Lysak thanks the reviewers for their assistance in evaluating this paper.

References

Abel, R. W., and R. M. Thorne (1998a), Electron scattering loss in Earth's inner magnetosphere: 1. Dominant physical processes, *J. Geophys. Res.*, *103*(A2), 2385–2396.

Abel, R. W., and R. M. Thorne (1998b), Electron scattering loss in Earth's inner magnetosphere: 2. Sensitivity to model parameters, *J. Geophys. Res.*, *103*(A2), 2397–2408.

Albert, J. M. (1994), Quasi-linear pitch angle diffusion coefficients: Retaining high harmonics, *J. Geophys. Res.*, *99*(A12), 23,741–23,745.

Angelopoulos, V. (2008), The THEMIS mission, *Space Sci. Rev.*, *141*, 5–34.

Angerami, J. J., and J. O. Thomas (1964), Studies of planetary atmospheres: 1. Distribution of electrons and ions in Earth's exosphere, *J. Geophys. Res.*, *69*(21), 4537–4560.

Bell, T. F., U. S. Inan, J. Bortnik, and J. D. Scudder (2002), The Landau damping of magnetospherically reflected whistlers within the plasmasphere, *Geophys. Res. Lett.*, *29*(15), 1733, doi:10.1029/2002GL014752.

Bespalov, P. A., M. Parrot, and J. Manninen (2010), Short-period VLF emissions as solitary envelope waves in a magnetospheric plasma maser, *J. Atmos. Sol. Terr. Phys.*, *72*(17), 1275–1281.

Bortnik, J., U. S. Inan, and T. F. Bell (2003), Energy distribution and lifetime of magnetospherically reflecting whistlers in the plasmasphere, *J. Geophys. Res.*, *108*(A5), 1199, doi:10.1029/2002JA009316.

Bortnik, J., R. M. Thorne, and N. P. Meredith (2007a), Modeling the propagation characteristics of chorus using CRRES suprathermal electron fluxes, *J. Geophys. Res.*, *112*, A08204, doi:10.1029/2006JA012237.

Bortnik, J., R. M. Thorne, N. P. Meredth, and O. Santolik (2007b), Ray tracing of penetrating chorus and its implications for the radiation belts, *Geophys. Res. Lett.*, *34*, L15109, doi:10.1029/2007GL030040.

Bortnik, J., R. M. Thorne, and N. P. Meredith (2008), The unexpected origin of plasmaspheric hiss from discrete chorus emissions, *Nature*, *452*(7183), 62–66.

Bortnik, J., W. Li, R. M. Thorne, V. Angelopoulos, C. Cully, J. Bonnell, O. Le Contel, and A. Roux (2009a), An observation linking the origin of plasmaspheric hiss to discrete chorus emissions, *Science*, *324*(5928), 775–778, doi:10.1126/science.1171273.

Bortnik, J., R. M. Thorne, and N. P. Meredith (2009b), Plasmaspheric hiss overview and relation to chorus, *J. Atmos. Sol. Terr. Phys.*, *71*(16), 1636–1646.

Boskova, J., F. Jiricek, P. Triska, B. V. Lundin, and D. R. Shklyar (1988), On the problem of quasi-electrostatic whistler mode waves: A possible interpretation of discrete plasmaspheric emissions, *Stud. Geophys. Geod.*, *32*(2), 199–212.

Brinca, A. L. (1972), On the stability of obliquely propagating whistlers, *J. Geophys. Res.*, *77*(19), 3495–3507.

Bud'ko, N. I. (1984), Generation of ELF hiss in the ionosphere by proton fluxes, *Geomagn. Aeron., Engl. Transl.*, *24*, 342–344.

Burtis, W. J., and R. A. Helliwell (1969), Banded chorus—A new type of VLF radiation observed in the magnetosphere by OGO 1 and OGO 3, *J. Geophys. Res.*, *74*(11), 3002–3010.

Burtis, W. J., and R. A. Helliwell (1976), Magnetospheric chorus: Occurrence patterns and normalized frequency, *Planet. Space Sci.*, *24*(11), 1007–1010.

Burton, R. K., and R. E. Holzer (1974), The origin and propagation of chorus in the outer magnetosphere, *J. Geophys. Res.*, *79*(7), 1014–1023.

Carpenter, D. L., and R. R. Anderson (1992), An ISEE/whistler model of equatorial electron density in the magnetosphere, *J. Geophys. Res.*, *97* (A2), 1097–1108.

Chan, K. W., and R. E. Holzer (1976), ELF hiss associated with plasma density enhancements in the outer magnetosphere, *J. Geophys. Res.*, *81* (13), 2267–2274.

Chen, L., J. Bortnik, R. M. Thorne, R. B. Horne, and V. K. Jordanova (2009), Three-dimensional ray tracing of VLF waves in a magnetospheric environment containing a plasmaspheric plume, *Geophys. Res. Lett.*, *36*, L22101, doi:10.1029/2009GL040451.

Chum, J., and O. Santolik (2005), Propagation of whistler-mode chorus to low altitudes: Divergent ray trajectories and ground accessibility, *Ann. Geophys.*, *23*, 3727–3738.

Church, S. R., and R. M. Thorne (1983), On the origin of plasmaspheric hiss: Ray path integrated amplification, *J. Geophys. Res.*, *88*(A10), 7941–7957.

Cornilleau-Wehrlin, N., R. Gendrin, F. Lefeuvre, M. Parrot, R. Grard, D. Jones, A. Bahnsen, E. Ungstrup, and W. Gibbons (1978), VLF electromagnetic waves observed onboard GEOS-1, *Space Sci. Rev.*, *22*, 371–382.

Denton, R. E., K. Takahashi, I. A. Galkin, P. A. Nsumei, X. Huang, B. W. Reinisch, R. R. Anderson, M. K. Sleeper, and W. J. Hughes (2006), Distribution of density along magnetospheric field lines, *J. Geophys. Res.*, *111*, A04213, doi:10.1029/2005JA011414.

Draganov, A. B., U. S. Inan, V. S. Sonwalkar, and T. F. Bell (1992), Magnetospherically reflected whistlers as a source of plasmaspheric hiss, *Geophys. Res. Lett.*, *19*(3), 233–236.

Draganov, A. B., U. S. Inan, V. S. Sonwalkar, and T. F. Bell (1993), Whistlers and plasmaspheric hiss: Wave directions and three-dimensional propagation, *J. Geophys. Res.*, *98*(A7), 11,401–11,410.

Dunckel, N., and R. A. Helliwell (1969), Whistler mode emissions on the OGO 1 satellite, *J. Geophys. Res.*, *74*(26), 6371–6385.

Ellis, G. R. A. (1959), Low frequency electromagnetic radiation associated with magnetic disturbances, *Planet. Space Sci.*, *1*(4), 253–254.

Etcheto, J., R. Gendrin, J. Solomon, and A. Roux (1973), A self-consistent theory of magnetospheric ELF hiss, *J. Geophys. Res.*, *78*(34), 8150–8166.

Goldstein, B. E., and B. T. Tsurutani (1984), Wave normal directions of chorus near the equatorial source region, *J. Geophys. Res.*, *89*(A5), 2789–2810.

Green, J. L., S. Boardsen, L. Garcia, W. W. L. Taylor, S. F. Fung, and B. W. Reinisch (2005), On the origin of whistler mode radiation in the plasmasphere, *J. Geophys. Res.*, *110*, A03201, doi:10.1029/2004JA010495.

Green, J. L., S. Boardsen, L. Garcia, W. W. L. Taylor, S. F. Fung, and B. W. Reinisch (2006), Reply to "Comment on "On the origin of whistler mode radiation in the plasmasphere" by Green et al.," *J. Geophys. Res.*, *111*, A09211,doi:10.1029/2006JA011622.

Gross, S. H. (1970), VLF duct associated with the lower-hybrid-resonance frequency in a multi-ion upper ionosphere, *J. Geophys. Res.*, *75*(22), 4235–4247.

Gross, S. H., and N. Larocca (1972), Phenomenological study of LHR hiss, *J. Geophys. Res.*, *77*(7), 1146–1156.

Gurnett, D. A., and B. J. O'Brien (1964), High-latitude geophysical studies with satellite Injun 3: 5. Very-low-frequency electromagnetic radiation, *J. Geophys. Res.*, *69*(1), 65–89.

Harang, L. (1968), VLF-emissions observed at stations close to the auroral zone and at stations on lower latitude, *J. Atmos. Terr. Phys.*, *30*(6), 1143–1160.

Hayakawa, M., and S. S. Sazhin (1992), Mid-latitude and plasmaspheric hiss: A review, *Planet. Space Sci.*, *40*(10), 1325–1338.

Hayakawa, M., Y. Tanaka, and J. Ohtsu (1975), The morphologies of low-latitude and auroral VLF "hiss," *J. Atmos. Terr. Phys.*, *37*(3), 517–529.

Hayakawa, M., K. Bullough, and T. R. Kaiser (1977), Properties of storm-time magnetospheric VLF emissions as deduced from the Ariel 3 satellite and ground-based observations, *Planet. Space Sci.*, *25*(4), 353–368.

Hayakawa, M., Y. Yamanaka, M. Parrot, and F. Lefeuvre (1984), The wave normals of magnetospheric chorus emissions observed onboard GEOS 2, *J. Geophys. Res.*, *89*(A5), 2811–2821.

Hayakawa, M., N. Ohmi, M. Parrot, and F. Lefeuvre (1986), Direction finding of ELF hiss emissions in a detached plasma region of the magnetosphere, *J. Geophys. Res.*, *91*(A1), 135–141.

Hayakawa, M., K. Hattori, S. Shimakura, M. Parrot, and F. Lefeuvre (1990), Direction finding of chorus emissions in the outer magnetosphere and their generation and propagation, *Planet. Space Sci.*, *38*(1), 135–143.

Horne, R. B. (1989), Path-integrated growth of electrostatic waves: The generation of terrestrial myriametric radiation, *J. Geophys. Res.*, *94* (A7), 8895–8909.

Huang, C. Y., and C. K. Goertz (1983), Ray-tracing studies and path-integrated gains of ELF unducted whistler mode waves in the Earth's magnetosphere, *J. Geophys. Res.*, *88*(A8), 6181–6187.

Huang, C. Y., C. K. Goertz, and R. R. Anderson (1983), A theoretical study of plasmaspheric hiss generation, *J. Geophys. Res.*, *88*(A10), 7927–7940.

Ichimaru, S. (1973), *Basic Principles of Plasma Physics: A Statistical Approach*, 324 pp., Benjamin, Reading, Mass.

Inan, U. S., and T. F. Bell (1977), The plasmapause as a VLF wave guide, *J. Geophys. Res.*, *82*(19), 2819–2827.

Katoh, Y., and Y. Omura (2007), Computer simulation of chorus wave generation in the Earth's inner magnetosphere, *Geophys. Res. Lett.*, *34*, L03102, doi:10.1029/2006GL028594.

Kennel, C. F. (1966), Low-frequency whistler mode, *Phys. Fluids*, *9*(11), 1958–1988.

Kennel, C. F., and H. E. Petschek (1966), Limit on stably trapped particle fluxes, *J. Geophys. Res.*, *71*(1), 1–28.

Kennel, C. F., and R. M. Thorne (1967), Unstable growth of unducted whistlers propagating at an angle to the geomagnetic field, *J. Geophys. Res.*, *72*(3), 871–878.

Kimura, I. (1966), Effects of ions on whistler-mode ray tracing, *Radio Sci.*, *1*(3), 269–283.

Kovner, M. S., V. A. Kuznetsova, and Y. I. Likhter (1978), Ionospheric generation of ELF radiation, *Geomagn. Aeron., Engl. Transl.*, *18*, 466–472.

Lam, M. M., R. B. Horne, N. P. Meredith, and S. A. Glauert (2007), Modeling the effects of radial diffusion and plasmaspheric hiss on outer radiation belt electrons, *Geophys. Res. Lett.*, *34*, L20112, doi:10.1029/2007GL031598.

Lampe, M., G. Joyce, W. M. Manheimer, and G. Ganguli (2010), Nonlinear whistler instability driven by a beamlike distribution of resonant electrons, *Phys. Plasmas*, *022902*, doi:10.1063/1.3298733.

Lauben, D. S., U. S. Inan, T. F. Bell, D. L. Kirchner, G. B. Hospodarsky, and J. S. Pickett (1998), VLF chorus emissions observed by Polar during the January 10, 1997, magnetic cloud, *Geophys. Res. Lett.*, *25*(15), 2995–2998.

Lauben, D. S., U. S. Inan, T. F. Bell, and D. A. Gurnett (2002), Source characteristics of ELF/VLF chorus, *J. Geophys. Res.*, *107*(A12), 1429, doi:10.1029/2000JA003019.

LeDocq, M. J., D. A. Gurnett, and G. B. Hospodarsky (1998), Chorus source locations from VLF Poynting flux measurements with the Polar spacecraft, *Geophys. Res. Lett.*, *25*(21), 4063–4066.

Lefeuvre, F., and R. A. Helliwell (1985), Characterization of the sources of VLF hiss and chorus observed on GEOS 1, *J. Geophys. Res.*, *90*(A7), 6419–6438.

Li, W., R. M. Thorne, N. P. Meredith, R. B. Horne, J. Bortnik, Y. Y. Shprits, and B. Ni (2008), Evaluation of whistler mode chorus amplification during an injection event observed on CRRES, *J. Geophys. Res.*, *113*, A09210, doi:10.1029/2008JA013129.

Li, W., R. M. Thorne, V. Angelopoulos, J. Bortnik, C. M. Cully, B. Ni, O. LeContel, A. Roux, U. Auster, and W. Magnes (2009), Global distribution of whistler-mode chorus waves observed on the THEMIS spacecraft, *Geophys. Res. Lett.*, *36*, L09104, doi:10.1029/2009GL037595.

Li, W., R. M. Thorne, J. Bortnik, Y. Nishimura, V. Angelopoulos, L. Chen, J. P. McFadden, and J. W. Bonnell (2010), Global distributions of suprathermal electrons observed on THEMIS and potential mechanisms for access into the plasmasphere, *J. Geophys. Res.*, *115*, A00J10, doi:10.1029/2010JA015687.

Lyons, L. R., and R. M. Thorne (1973), Equilibrium structure of radiation belt electrons, *J. Geophys. Res.*, *78*(13), 2142–2149.

Lyons, L. R., R. M. Thorne, and C. F. Kennel (1972), Pitch-angle diffusion of radiation belt electrons within the plasmasphere, *J. Geophys. Res.*, *77* (19), 3455–3474.

McFadden, J. P., C. W. Carlson, D. Larson, M. Ludlam, R. Abiad, B. Elliott, P. Turin, M. Marckwordt, and V. Angelopoulos (2008), The THEMIS ESA plasma instrument and in-flight calibration, *Space Sci. Rev.*, *141*, 277–302.

Meredith, N. P., R. B. Horne, and R. R. Anderson (2001), Substorm dependence of chorus amplitudes: Implications for the acceleration of electrons to relativistic energies, *J. Geophys. Res.*, *106*(A7), 13,165–13,178.

Meredith, N. P., R. B. Horne, R. M. Thorne, and R. R. Anderson (2003), Favored regions for chorus-driven electron acceleration to relativistic energies in the Earth's outer radiation belt, *Geophys. Res. Lett.*, *30*(16), 1871, doi:10.1029/2003GL017698.

Meredith, N. P., R. B. Horne, R. M. Thorne, D. Summers, and R. R. Anderson (2004), Substorm dependence of plasmaspheric hiss, *J. Geophys. Res.*, *109*, A06209, doi:10.1029/2004JA010387.

Meredith, N. P., R. B. Horne, M. A. Clilverd, D. Horsfall, R. M. Thorne, and R. R. Anderson (2006), Origins of plasmaspheric hiss, *J. Geophys. Res.*, *111*, A09217, doi:10.1029/2006JA011707.

Meredith, N. P., R. B. Horne, S. Glauert, and R. R. Anderson (2007), Slot region electron loss timescales due to plasmaspheric hiss and lightning generated whistlers, *J. Geophys. Res.*, *112*, A08214, doi:10.1029/2007JA012413.

Molchanov, O. A., M. Parrot, M. M. Mogilevski, and F. Lefeuvre (1991), A theory of PLHR emissions to explain the weekly variation of ELF data observed by a low-latitude satellite, *Ann. Geophys.*, *9*, 669–680.

Nunn, D. (1971), A theory of VLF emissions, *Planet. Space Sci.*, *19*(9), 1141–1167.

Nunn, D. (1974), A self-consistent theory of triggered VLF emissions, *Planet. Space Sci.*, *22*(3), 349–378.

Nunn, D., O. Santolik, M. Rycroft, and V. Trakhtengerts (2009), On the numerical modelling of VLF chorus dynamical spectra, *Ann. Geophys.*, *27*, 2341–2359.

Omura, Y., Y. Katoh, and D. Summers (2008), Theory and simulation of the generation of whistler-mode chorus, *J. Geophys. Res.*, *113*, A04223, doi:10.1029/2007JA012622.

Omura, Y., M. Hikishima, Y. Katoh, D. Summers, and S. Yagitani (2009), Nonlinear mechanisms of lower-band and upper-band VLF chorus emissions in the magnetosphere, *J. Geophys. Res.*, *114*, A07217, doi:10.1029/2009JA014206.

Ondoh, T., Y. Nakamura, S. Watanabe, K. Aikyo, and T. Murakami (1980), Narrow-band VLF kHz hiss observed in the vicinity of the plasmapause, *J. Radio Res. Lab. Jpn.*, *27*, 131–140.

Ondoh, T., Y. Nakamura, S. Watanabe, and T. Murakami (1981), Narrow-band 5 kHz hiss observed in the vicinity of the plasmapause, *Planet. Space Sci.*, *29*(1), 65–72.

Ondoh, T., Y. Nakamura, S. Watanabe, K. Aikyo, and T. Murakami (1982), Plasmaspheric ELF hiss observed by ISIS satellites, *J. Radio Res. Lab. Jpn.*, *29*, 159–181.

Ondoh, T., Y. Nakamura, S. Watanabe, K. Aikyo, and T. Murakami (1983), Plasmaspheric hiss observed in the topside ionosphere at mid- and low-latitudes, *Planet. Space Sci.*, *31*(4), 411–422.

Parady, B. K. (1974), Anisotropic proton instability for magnetospheric (APIM) hiss: An introduction, *Geophys. Res. Lett.*, *1*(6), 235–238.

Parrot, M., and F. Lefeuvre (1986), Statistical study of the propagation characteristics of ELF hiss observed on GEOS-1, inside and outside the plasmasphere, *Ann. Geophys., Ser. A*, *4*, 363–384.

Parrot, M., O. A. Molchanov, M. M. Mogilevski, and F. Lefeuvre (1991), Daily variations of ELF data observed by a low-altitude satellite, *Geophys. Res. Lett.*, *18*(6), 1039–1042.

Parrot, M., O. Santolik, D. Gurnett, J. Pickett, and N. Cornilleau-Wehrlin (2004), Characteristics of magnetospherically reflected chorus waves observed by Cluster, *Ann. Geophys.*, *22*, 2597–2606.

Russell, C. T., R. E. Holzer, and E. J. Smith (1969), OGO 3 observations of ELF noise in the magnetosphere: 1. Spatial extent and frequency of occurrence, *J. Geophys. Res.*, *74*(3), 755–777.

Santolik, O., and D. A. Gurnett (2003), Transverse dimensions of chorus in the source region, *Geophys. Res. Lett.*, *30*(2), 1031, doi:10.1029/2002GL016178.

Santolik, O., D. A. Gurnett, J. S. Pickett, M. Parrot, and N. Cornilleau-Wehrlin (2003), Spatio-temporal structure of storm-time chorus, *J. Geophys. Res.*, *108*(A7), 1278, doi:10.1029/2002JA009791.

Santolik, O., D. A. Gurnett, and J. S. Pickett (2004), Multipoint investigation of the source region of storm-time chorus, *Ann. Geophys.*, *22*, 2555–2563.

Santolik, O., D. A. Gurnett, J. S. Pickett, M. Parrot, and N. Cornilleau-Wehrlin (2005), Central position of the source region of storm-time chorus, *Planet. Space Sci.*, *53*(1–3), 299–305.

Santolik, O., J. Chum, M. Parrot, D. A. Gurnett, J. S. Pickett, and N. Cornilleau-Wehrlin (2006), Propagation of whistler mode chorus to low altitudes: Spacecraft observations of structured ELF hiss, *J. Geophys. Res.*, *111*, A10208, doi:10.1029/2005JA011462.

Santolik, O., D. A. Gurnett, J. S. Pickett, J. Chum, and N. Cornilleau-Wehrlin (2009), Oblique propagation of whistler mode waves in the chorus source region, *J. Geophys. Res.*, *114*, A00F03, doi:10.1029/2009JA014586.

Santolik, O., et al. (2010), Wave-particle interactions in the equatorial source region of whistler-mode emissions, *J. Geophys. Res.*, *115*, A00F16, doi:10.1029/2009JA015218.

Sazhin, S. S. (1984), A model for hiss-type mid-latitude VLF emissions, *Planet. Space Sci.*, *32*(10), 1263–1271.

Sazhin, S. S. (1989), Improved quasilinear models of parallel whistler-mode instability, *Planet. Space Sci.*, *37*(6), 633–647.

Sazhin, S. S. (2005), *Whistler-Mode Waves in a Hot Plasma*, Cambridge Univ. Press, Cambridge, U. K.

Schriver, D., et al. (2010), Generation of whistler mode emissions in the inner magnetosphere: An event study, *J. Geophys. Res.*, *115*, A00F17, doi:10.1029/2009JA014932.

Shklyar, D., and H. Matsumoto (2009), Oblique whistler-mode waves in the inhomogeneous magnetospheric plasma: Resonant interactions with energetic charged particles, *Surv. Geophys.*, *30*(2), 55–104, doi:10.1007/s10712-009-9061-7.

Smith, E. J., A. M. A. Frandsen, B. T. Tsurutani, R. M. Thorne, and K. W. Chan (1974), Plasmaspheric hiss intensity variations during magnetic storms, *J. Geophys. Res.*, *79*(16), 2507–2510.

Smith, R. L., I. Kimura, J. Vigneron, and J. Katsufrakis (1966), Lower hybrid resonance noise and a new ionospheric duct, *J. Geophys. Res.*, *71*(7), 1925–1927.

Sonwalkar, V. S., and U. S. Inan (1989), Lightning as an embryonic source of VLF hiss, *J. Geophys. Res.*, *94*(A6), 6986–6994.

Stenzel, R. L. (1976), Antenna radiation patterns in the whistler wave regime measured in a large laboratory plasma, *Radio Sci.*, *11*(12), 1045–1056.

Stix, T. H. (1992), *Waves in Plasmas*, Am. Inst. of Phys., New York.

Storey, L. R. O., F. Lefeuvre, M. Parrot, L. Cairo, and R. Anderson (1991), Initial survey of the wave distribution functions for plasmaspheric hiss observed by ISEE 1, *J. Geophys. Res.*, *96*(A11), 19,469–19,489.

Stringer, T. E. (1963), Low frequency waves in an unbound plasma, *J. Nucl. Energy, Part C*, *5*, 89–107.

Summers, D., and R. M. Thorne (1991), The modified plasma dispersion function, *Phys. Fluids B*, *3*, 1835–1847.

Summers, D., B. Ni, and N. P. Meredith (2007), Timescales for radiation belt electron acceleration and loss due to resonant wave particle interactions: 2. Evaluation for VLF chorus, ELF hiss, and EMIC waves, *J. Geophys. Res.*, *112*, A04207, doi:10.1029/2006JA011993.

Summers, D., B. Ni, N. P. Meredith, R. B. Horne, R. M. Thorne, M. B. Moldwin, and R. R. Anderson (2008), Electron scattering by whistler-mode ELF hiss in plasmaspheric plumes, *J. Geophys. Res.*, *113*, A04219, doi:10.1029/2007JA012678.

Swanson, D. G. (1989), *Plasma Waves*, Academic, New York.

Thorne, R. M., and C. F. Kennel (1967), Quasi-trapped VLF propagation in the outer magnetosphere, *J. Geophys. Res.*, *72*(3), 857–870.

Thorne, R. M., E. J. Smith, R. K. Burton, and R. E. Holzer (1973), Plasmaspheric hiss, *J. Geophys. Res.*, *78*(10), 1581–1595.

Thorne, R. M., E. J. Smith, K. J. Fiske, and S. R. Church (1974), Intensity variation of ELF hiss and chorus during isolated substorms, *Geophys. Res. Lett.*, *1*(5), 193–196.

Thorne, R. M., S. R. Church, W. J. Malloy, and B. T. Tsurutani (1977), The local time variation of ELF emissions during periods of substorm activity, *J. Geophys. Res.*, *82*(10), 1585–1590.

Thorne, R. M., S. R. Church, and D. J. Gorney (1979), On the origin of plasmaspheric hiss: The importance of wave propagation and the plasmapause, *J. Geophys. Res.*, *84*(A9), 5241–5247.

Thorne, R. M., R. B. Horne, and N. P. Meredith (2006), Comment on "On the origin of whistler mode radiation in the plasmasphere" by Green et al., *J. Geophys. Res.*, *111*, A09210, doi:10.1029/2005JA011477.

Trakhtengerts, V. Y., M. J. Rycroft, and A. G. Demekhov (1996), Interrelation of noise-like and discrete ELF/VLF emissions generated by cyclotron interactions, *J. Geophys. Res.*, *101*(A6), 13,293–13,301, doi:10.1029/95JA03515.

Trakhtengerts, V. Y., A. G. Demekhov, E. E. Titova, B. V. Kozelov, O. Santolik, D. Gurnett, and M. Parrot (2004), Interpretation of Cluster data on chorus emissions using the backward wave oscillator model, *Phys. Plasmas*, *11*, 1345–1351.

Tsurutani, B. T., and E. J. Smith (1974), Postmidnight chorus: A substorm phenomenon, *J. Geophys. Res.*, *79*(1), 118–127.

Tsurutani, B. T., O. P. Verkhoglyadova, G. S. Lakhina, and S. Yagitani (2008), Properties of dayside outer zone chorus during HILDCAA events: Loss of energetic electrons, *J. Geophys. Res.*, *114*, A03207, doi:10.1029/2008JA013353.

J. Bortnik, L. Chen, W. Li, and R. M. Thorne, Department of Atmospheric and Oceanic Sciences, University of California, Los Angeles, CA 90095-1565, USA. (jbortnik@atmos.ucla.edu; clj@atmos.ucla.edu; moonli@atmos.ucla.edu; rmt@atmos.ucla.edu)

R. B. Horne, British Antarctic Survey, Madingley Road, Cambridge CB3 0ET, UK. (rh@bas.ac.uk)